

Hand-Held Sound-Speed Imaging Based on Ultrasound Reflector Delineation

Sergio J. Sanabria^(✉) and Orcun Goksel

Computer-assisted Applications in Medicine, ETH Zurich, Zurich, Switzerland
ssanabria@ethz.ch

Abstract. A novel hand-held speed-of-sound (SoS) imaging method is proposed, which requires only minor hardware extensions to conventional ultrasound (US) B-mode systems. A hand-held reflector is used as a timing reference for US signals. A robust reflector-detection algorithm, based on *dynamic programming* (DP), achieves unambiguous timing even with 10 dB signal-to-noise ratio in real tissues, successfully detecting delays <100 ns introduced by SoS heterogeneities. An *Anisotropically-Weighted Total-Variation* (AWTV) regularization based on L1-norm smoothness reconstruction is shown to achieve significant improvements in the delineation of focal lesions. The Contrast-to-noise-ratio (CNR) is improved from 15 dB to 37 dB, and the axial resolution loss from $>300\%$ to $<15\%$. Experiments with breast-mimicking phantoms and *ex-vivo* liver samples showed, for hard hypoechogenic inclusions not visible in B-mode US, a high SoS contrast (2.6 %) with respect to cystic inclusions (0.9 %) and the background SoS noise (0.6 %). We also tested our method on a healthy volunteer in a preliminary *in-vivo* test. The proposed technique demonstrates potential for low-cost and non-ionizing screening, as well as for diagnostics in daily clinical routine.

1 Introduction

Breast cancer is a high-prevalence disease affecting 1/8 women in the USA. Current routine screening consists of X-ray mammography, which, however, shows low sensitivity to malign tumors in dense breasts, for which a large number of false positives leads to an unnecessary number of breast biopsies. Also, the use of ionizing radiation advises against a frequent utilization, for instance, to monitor the progress of a tumor. Finally, the compression of the breast down to a few centimeter may cause patient discomfort. For these reasons, latest recommendations restrict the general use of X-ray mammography to biennial examinations in women over 50 year old [13].

Ultrasound (US) is a safe, pain-free, and widely available medical imaging modality, which can complement routine mammographies. Conventional screening breast US (B-mode), which measures reflectivity and scattering from tissue structures, showed significantly higher sensitivity combined with mammography (97 %) than the latter alone (74 %) [8]. However, B-mode US shows poor specificity. A novel US modality, Ultrasound Computed-tomography (USCT), aims at

mapping other tissue parameters, such as the speed-of-sound (SoS), which shows a high potential for tumor differentiation (e.g., fibroadenoma, carcinoma, cysts) [2]. However, this method requires dedicated and complex systems consisting of a large number of transducer elements located around the breast in order to measure US wave propagation paths along multiple trajectories, from which the SoS-USCT image is reconstructed [3, 5, 10, 11]. Low-cost extensions of conventional B-mode systems that only require a single multi-element array transducer are desirable for SoS-USCT for the daily clinical routine. There have been some early attempts to combine B-mode systems with X-ray mammography, using the back compression plate as a timing reference. Yet, the reconstruction suffers from strong limited-angle artifacts, which provide unsatisfactory image quality, unless detailed prior information of the screened inclusion geometry is available [6, 9].

In this work we propose a novel SoS-USCT method, *hand-held sound-speed imaging*, which overcomes the above listed limitations. By transmitting US waves through tissue between a B-mode transducer and a hand-held reflector, a SoS-USCT image of sufficient quality for tumor screening is obtained (Fig. 1). A specific reflector design combined with dedicated image processing provides unambiguous measurement of US time-of-flight (ToF) between different transmitter/receiver elements of a transducer, from which local tissue SoS is derived as an image.

Total-variation regularization overcomes the previously reported limited-angle artifacts and enables prior-less SoS imaging and precise delineation of piece-wise homogeneous inclusions. The proposed method only requires a small and localized breast compression, while allowing for flexible access to arbitrary imaging planes within the breast.

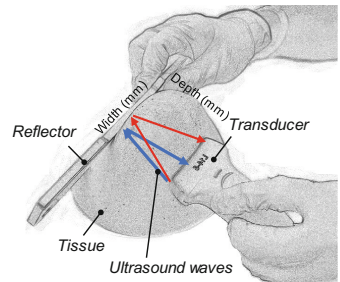


Fig. 1. SoS imaging setup.

2 Methods

A 128-element 5 MHz linear ultrasound array (L14/5-38) was operated in multistatic mode (a), each element sequentially fringing (Tx) and the rest receiving (Rx). For this purpose, a custom acquisition sequence was implemented on a research ultrasound machine (SonixTouch, Ultrasonix, Richmond, Canada). In a first implementation, a conventional ultrasound beamformer is adapted to the application by beamforming only a single element pair in Tx and Rx at a time, which requires the acquisition of 128×128 RF lines for 40 mm depth in about 8 s. To keep the measurement scene stable during acquisition, a positioning frame was introduced to keep the orientation of transducer and reflector fixed with respect to each other (Fig. 5b). For each line, the raw (unmodulated) ultrasound data (RF lines) are recorded. Computations are then performed in Matlab[®].

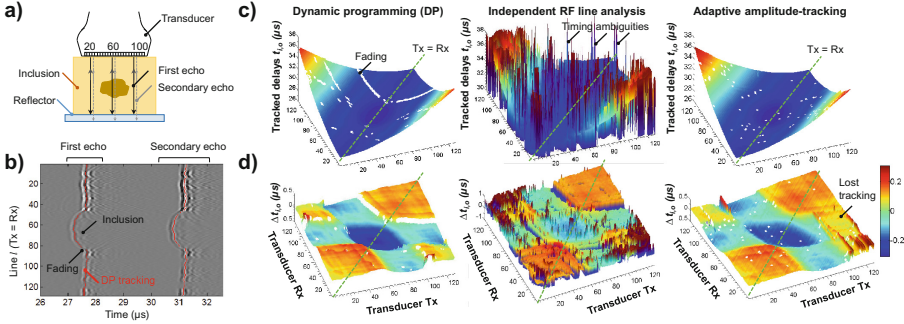


Fig. 2. Reflector identification for *ex-vivo* liver test (Fig. 5c). a) Setup details; b) RF lines acquired with overlapped DP delineation for the case of same Tx and Rx; c) the measured ToF matrix $t_{i,o}$; and d) the relative path delays $\Delta t_{i,o}$ after compensating for geometric effects. The proposed DP method outperforms independent RF line analysis and adaptive amplitude-tracking [12].

2.1 Reflector Delineation

The reflector consists of a thin Plexiglas stripe (50 mm × 7 mm × 5 mm), which limits the reflected echoes to the desired imaging plane, and allows for flexible access to different breast locations. The material choice ensures a coherent wave reflection along the tested angular range. The flat reflector geometry is simple for manufacture, and easy to identify in US data. Secondary echoes corresponding to wave reflections between reflector boundaries are well-separated from the main echo and filtered out (Fig. 2a, b).

In a real tissue scenario, a modulated ultrasound waveform with an oscillatory pressure pattern is recorded. The recorded signal shows multiple local maxima, with varying amplitudes depending on the wave path. Simply picking the peak response in each RF line yields incorrect ToF values, since different peaks may be selected for different transmit-receive (Tx-Rx) pairs. An adaptive amplitude-tracking measurement, which uses the current timing measurement as prior information for the adjacent Tx-Rx pairs, was shown for non-destructive testing of heterogeneous materials [12]. However, it requires manual initialization, which is not affordable for *in-vivo* scenarios and fails when, due to wave interference and scattering effects, the reflected wave-front falls below the system noise level (fading), as frequently observed in real tissue samples (Fig. 2c, d).

In this work a global optimization is introduced, which simultaneously considers the full Tx-Rx dataset. Based on Dynamic Programming (DP), which has been applied in US for the segmentation of bones [4] and vessel walls [1], an algorithm for detecting oscillatory patterns in RF lines is proposed. It consists of a global cost matrix $C(l, t_l)$, which is cumulatively built along successive RF lines l (adjacent Tx-Rx pairs) for a list of N timing candidates $t_l = t_l^0, t_l^1 \dots t_l^N$, i.e., a list of possible time samples in the current RF line l , among which the optimum reflector timing can be found. Also, a memory matrix $M(l, t_l)$ records

discrete timing decisions for each line and candidate. The optimum reflector timing is then found, which minimizes the cumulative cost, and following $M(l, t_l)$ backwards the optimum reflector delineation $T(l)$ is drawn:

$$\begin{aligned} \begin{pmatrix} C(l, t_l) \\ M(l, t_l) \end{pmatrix} &= \begin{pmatrix} \min_{t_{l-1}} \{C(l-1, t_{l-1}) + f_1(t_l, t_{l-1})\} + f_0(t_l) \\ \operatorname{argmin}_{t_{l-1}} \{C(l-1, t_{l-1}) + f_1(t_l, t_{l-1})\} \end{pmatrix} \\ T(l) &= \begin{cases} \operatorname{argmin}_{t_l} C(l, t_l), & l = L; \\ M(l+1, T(l+1)), & l = 1 \dots L-1; \end{cases} \end{aligned} \quad (1)$$

with f_0 and f_1 non-linear functions that incorporate ToF for current t_l and neighbouring t_{l-1} RF lines. The general formulation of Eq. 1 introduces regularization into the reflector timing problem, enabling the natural incorporation of available prior information (oscillatory pattern, smoothness, multiple echoes, path geometry) into the optimization. Moreover, the delineation does not require manual initialization and is parallelizable linewise. The currently not optimized Matlab code runs on a single-core of an Intel Core i7-4770K CPU in <100 s, but several future speed improvements are envisioned.

2.2 Total-Variation Sound-Speed Image Reconstruction

Once the time delay matrix for all transmit-receiver elements $t_{i,o}$ has been obtained (Fig. 2c), a SoS image is reconstructed. First, the baseline geometrical delays $\bar{t}_{i,o}$ due to different path lengths between different transmit-receiver elements are subtracted from $t_{i,o}$ to isolate the relative delays induced by SoS inhomogeneities $\Delta t_{i,o}$ (Fig. 2d):

$$\Delta t_{i,o} = t_{i,o} - \bar{t}_{i,o} \quad \bar{t}_{i,o} = (\bar{c})^{-1} \sqrt{4d^2 + p(i_o - i_i)^2} \quad \forall i, o \quad (2)$$

where \bar{c} is the average tissue speed of sound (with a nominal value of 1540 ms⁻¹), d is the distance between transducer and reflector, p is array pitch (0.3 mm for our probe), and i_i, i_o are the indices of the Tx i and Rx o elements considered (1..128). Note that d and \bar{c} are estimated with linear regression based on Eq. 2. In practice, a non-linear fit is performed to estimate both the reflector inclination and in-plane orientation.

The next step is the reconstruction of SoS distribution, which is expressed in slowness units σ [s/m], with $c(x, y) = \bar{c}(1 + \sigma(x, y))^{-1}$. The tissue region is discretized into cells c traversed by a finite set of ray paths p corresponding to different Tx-Rx pairs (Fig. 3a). With the known differential path lengths $l_{p,c}$, the path delays Δt_p are calculated in function of the slowness increments σ_c , i.e., $\Delta t_p = \sum_{c=1}^C l_{p,c} \sigma_c$, in matrix form $\Delta \mathbf{t} = \mathbf{L} \boldsymbol{\sigma}$. Since reconstruction can be ill-posed, regularization becomes necessary. A conventional solution in X-ray Computed Tomography (CT) [7], is *Filtered Backprojection (FBP)*, which averages the delays of all rays p propagating through cell c . Previous reflector-based US works [9] have used *Algebraic Reconstruction (ART)*, in which $\Delta \mathbf{t} = \mathbf{L} \boldsymbol{\sigma}$ is approximated via singular value decomposition, preserving only the largest singular values of \mathbf{L} (typically 5 % of the total). Both FBP and ART provide a stable

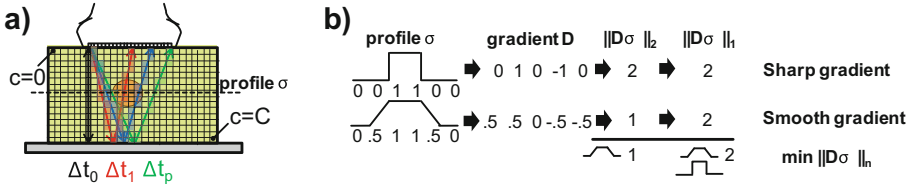


Fig. 3. Formulation of the sound-speed reconstruction problem. (a) Ray tracing discretization. (b) Smoothness regularization with L2 and L1 norms. While the L2 norm favors the smooth sound-speed profile, the L1 norm (TV) equally weights smooth and sharp gradients.

SoS-image reconstruction, which however suffers from strong streak artifacts and a coarse resolution in the vertical direction (Fig. 4c). The reason is that, similarly as in limited-angle CBCT, reflector-based SoS-USCT is an ill-posed problem [7], every cell being traversed by only a limited set of path orientations; i.e., paths parallel to the reflector are missing. This is a main geometric limitation with respect to dedicated USCT systems, which incorporate complete angular path sets [3, 5, 10].

To overcome the limited-angle artifacts, we introduce additional regularizing assumptions for the smoothness of the SoS-image:

$$\hat{\sigma}_{TV} = \operatorname{argmin}_{\sigma} \{ \|\Delta \mathbf{t} - \mathbf{L}\sigma\|_2 + \lambda \|\mathbf{D}\sigma\|_n \} \quad (3)$$

where $\|\mathbf{D}\sigma\|_n = \sum_{i,j} |\sigma_{i+1,j} - \sigma_{i,j}|^n + |\sigma_{i,j+1} - \sigma_{i,j}|^n$ minimizes the sum of horizontal i and vertical j gradients of the reconstructed image, and λ is a constant. The norm of the smoothness term n critically influences the reconstruction results (Fig. 3b). For L2-norm, i.e., $\|\mathbf{x}\|_2 = \sum |x|^2$, a closed linear solution (Tikhonov regularization) of Eq. 3 is found, but smooth gradients are favored with respect to sharp gradients. As a result, the reconstruction does not significantly improve with respect to ART. However, if the L1-norm $n = 1$ is

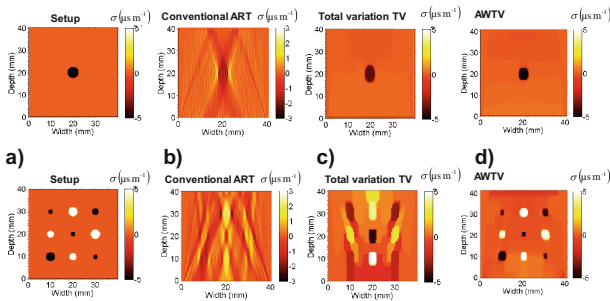


Fig. 4. Simulation of sound-speed image reconstruction with (top) single and (bottom) multiple inclusions: (a) in-silico phantom, (b-c) reconstruction with prior-art, and (d) our TV approach.

used $\|\mathbf{x}\|_1 = \sum |x|$ (*Total Variation (TV) Regularization*), sharp and smooth gradients are equally weighted, which leads to the reconstruction of a minimum number of piecewise homogeneous inclusions. This concept has been previously applied to regularize sparse array apertures in full-angle 3D USCT [11]. We apply this here for the first time to the limited-angle ultrasound reflection tomography case. With $n = 1$, Eq. 3 becomes a convex problem, which is iteratively solved with off-the-shelf optimization packages.

The resulting SoS images (Fig. 4c) successfully filter out limited-angle artifacts and delineate closed inclusion geometries. However, they still show reduced axial resolution, due to the extremely reduced path orientation set (according to Fig. 3a, for a SoS image aspect ratio of 1:1, the largest available ray angle is 25°). In order to compensate for this resolution loss we introduce *Anisotropically-Weighted Total Variation* (AWTV), which balances horizontal and vertical gradients with a constant κ according to the available ray information in each direction:

$$\hat{\sigma}_{\text{AWTV}} = \underset{\sigma}{\operatorname{argmin}} \left\{ \|\Delta \mathbf{t} - \mathbf{L}\sigma\|_2 + \lambda \sum_{i,j} \kappa |\sigma_{i+1,j} - \sigma_{i,j}| + (1 - \kappa) |\sigma_{i,j+1} - \sigma_{i,j}| \right\} \quad (4)$$

With a reconstructed pixel size equal to the array pitch ($p = 0.3$ mm), an optimum reconstruction performance was achieved with $\lambda = 0.0008$ and $\kappa = 0.9$.

2.3 Tissue Phantoms, *Ex-vivo* and *In-vivo* Tests

A tissue-mimicking phantom was manufactured from gelatin (9 g/100 mL water), mixed with flour to simulate typical ultrasound reflectivity patterns (speckle). Hard inclusions simulating tumors (Fig. 5a) were introduced by using a higher amount of gelatin (13 g/100 mL water) in well-defined phantom regions. In order to make these inclusions invisible to conventional B-mode US, the same amount of scattering was used in tissue background and hard inclusions, so that both exhibited the same echogenicity. To test the applicability of the method to breast mammography, a breast elastography phantom (Model 059, CIRS Inc., Norfolk, VA, USA) was tested. The phantom is fabricated with a tissue-mimicking material (ZerdineTM) and shows a realistic breast geometry, incorporating both skin layers and glandular tissue, together with cystic (water) and dense lesions (with embedded microcalcifications) (Fig. 5b). *Ex-vivo* tests were performed in bovine liver samples. Hard inclusions were simulated by ablating small pieces of liver (submerged in 250 mL water for 6 min at 700 W microwave). These were afterwards inserted in the liver (Fig. 5c). Finally, a preliminary *in-vivo* test was carried out with a healthy volunteer with benign cysts. While the subject sat in tripod position (Fig. 5d), the sonographer placed the US probe on the region-of-interest. Then, the subject held the positioning frame closed with both hands, while the reflector USCT data was acquired. For all tests, B-mode US images were also generated from the multi-static datasets for comparison with the SoS images.

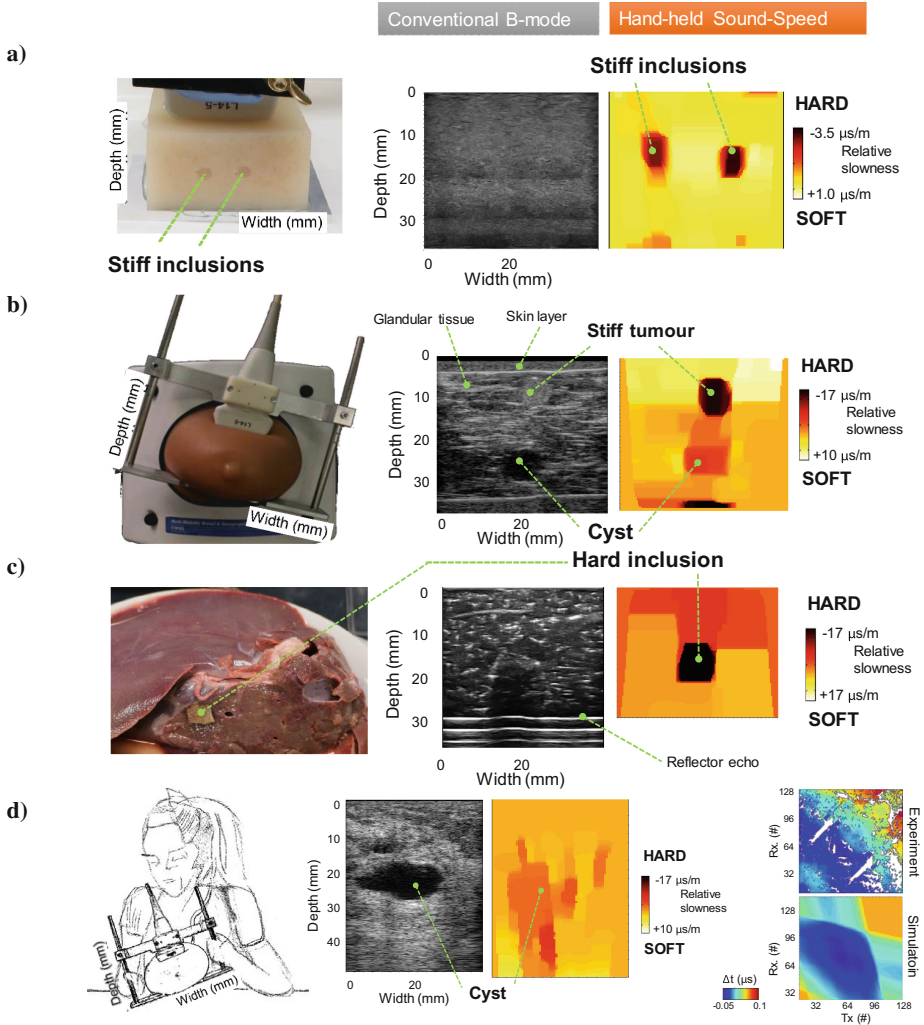


Fig. 5. Hand-held sound-speed mammography of gelatin phantom (a), breast-mimicking phantom (b), *ex-vivo* liver sample with hard inclusion (c), and *in-vivo* data for a benign cystic mass (d).

3 Results and Discussion

The proposed DP method clearly outperforms independent RF line analysis and adaptive amplitude-tracking, enabling the acquisition of a continuous ToF matrix for real tissues (Fig. 2c), in which small timing variations (<100 ns) caused by SoS inhomogeneities are successfully observed (Fig. 2d). Signal fading (Fig. 2b) was typically observed around the inclusion boundaries, where strong wave refraction occurs due to quasi-parallel incident ray paths. DP automati-

cally filters out fading positions from the reconstruction. Calibration experiments in gradually-heated water provided quantitative SoS values with a sensitivity $< 0.005 \text{ ms}^{-1}$. The observed timing error of $\text{std} = 15 \text{ ns}$ results in a noise floor of $0.8 \text{ } \mu\text{s m}^{-1}$, corresponding to a $< 0.1\%$ sound-speed contrast.

The proposed AWTV SoS reconstruction achieves significant improvements in the delineation of inclusion geometry (Fig. 4). Often-problematic vertical elongation of inclusions is strongly reduced (14%) compared to ART ($> 300\%$) and TV (95%), which enables a *quantitative* reconstruction of original SoS values (SoS error $< 0.3\%$). Streak artifacts, which are typical in ART (CNR = 15 dB), are not visible in AWTV (CNR = 37 dB). Moreover, our novel approach successfully reconstructs multiple inclusions with different SoS values and geometries (Fig. 4). Not only are the inclusion positions correctly identified, but also are their SoS values and diameter satisfactorily estimated.

An excellent performance is observed in both phantom and *ex-vivo* tests. For the gelatin phantom, the hard inclusions were manufactured with a small SoS contrast ($-3.5 \text{ } \mu\text{s m}^{-1}$, 0.5% SoS increase), but nonetheless were successfully resolved (Fig. 5a). In the more heterogeneous breast phantom (Fig. 5b) both hard inclusions ($-17 \text{ } \mu\text{s m}^{-1}$, 2.6% SoS increase) and cysts ($-6 \text{ } \mu\text{s m}^{-1}$, 0.9% SoS increase) show a higher contrast and are well-separated from the background noise, which is around 0.6%. These values are more representative of real breast tumors, as reported by [2]. The background noise is related to reconstruction artifacts (e.g., the gradient information is missing at image boundaries), and to a minor extent, to refraction effects not accounted for in the ray tracing model. The hard inclusion in the *ex-vivo* liver samples was invisible in the B-mode, but clearly delineated in the SoS image, with contrast similar to the breast phantom; see Fig. 5d. Despite movement artifacts, lower US signal-to-noise ratio ($< 10 \text{ dB}$), and imperfect coupling between reflector and breast tissue, the preliminary *in-vivo* test demonstrates a successful identification of cystic inclusion, with an expected lower SoS contrast ($-8 \text{ } \mu\text{s m}^{-1}$) than the *ex-vivo* hard inclusions.

4 Conclusions and Outlook

A novel hand-held sound-speed imaging modality has been proposed with minimum hardware modifications to conventional B-mode ultrasound systems. An accurate geometric delineation of hypoechogenic inclusions was achieved with a high SoS-contrast for hard inclusions in both breast elastography phantoms and *ex-vivo* liver samples. SoS values are known as potential quantitative imaging biomarkers for breast mass differentiation [2]. In our preliminary *in-vivo* test, even cystic inclusion, which are known to be of low SoS contrast, were successfully identified, indicating the future potential for detecting higher contrast cancerous tumors. The proposed method is radiation-free, painless, and can potentially complement routine screening for breast cancer. Prospective applications can be for other organs that allow reflector placement such as the testicles, limbs, skin, the prostate, and with catheters; or during open-surgery, e.g., for liver.

Acknowledgment. This work was funded by the Swiss National Science Foundation.

References

1. Crimi, A., Makhinya, M., Baumann, U., Thalhammer, C., et al.: Automatic measurement of venous pressure using B-mode ultrasound. *IEEE TMI* **63**, 288–299 (2016)
2. Duric, N., Littrup, P., Li, C., Roy, O., Schmidt, S., et al.: Breast imaging with softVue: initial clinical examination. In: *SPIE Medical Imaging*, pp. 90400V (2014)
3. Duric, N., Littrup, P., Poulo, L., Babkin, A., Pevzner, R., Holsapple, E.: Detection of breast cancer with ultrasound tomography: first results with the computer ultrasound risk evaluation (cure) prototype. *Med. Phys.* **34**, 773–785 (2007)
4. Foroughi, P., Boctor, E., et al.: Ultrasound bone segmentation using dynamic programming. In: *IEEE Ultras Symposium*, New York, NY, USA, pp. 2523–2526 (2007)
5. Gemmeke, H., Ruiter, N.V.: 3D ultrasound computer tomography for medical imaging. *Nucl. Instrum. Methods Phys. Res. A* **580**, 1057–1065 (2007)
6. Huang, S.W., Pai-Chi, L.: Ultrasonic computed tomography reconstruction of the attenuation coefficient using a linear array. *IEEE TUFFC* **52**, 2011–2022 (2005)
7. Kak, A.C., Slaney, M.: *Principles of computerized tomographic imaging*. IEEE Press, New York (1988)
8. Kolb, T.M., Lichy, J., Newhouse, J.H.: Comparison of the performance of screening mammography, physical examination, and breast us and evaluation of factors that influence them: an analysis of 27,825 patient evaluation. *Radiology* **225**, 165–175 (2002)
9. Krueger, M., Burow, V., et al.: Limited-angle us transmission tomography of the compressed female breast. In: *IEEE Ultrasonics Symposium*, Miyagi, Japan, pp. 1345–1348 (1998)
10. Nebeker, J., Nelson, T.R.: Imaging of sound speed using reflection ultrasound tomography. *J. Ultrasound Med.* **31**, 1389–1404 (2012)
11. Radovan, J., Peterlik, I., et al.: Sound-speed image reconstruction in sparse-aperture 3-D us transmission tomography. *IEEE Trans. Ultrason. Ferroelectr., Freq. Control* **59**, 254–264 (2012)
12. Sanabria, S.J., Hilbers, U., et al.: Modeling and prediction of density distribution and microstructure in particleboards from acoustic properties by correlation of non-contact high-resolution pulsed air-coupled ultrasound and X-ray images. *Ultrasonics* **53**, 157–170 (2013)
13. Siu, A., U.S. Preventive Services Task Force: Screening for breast cancer: U.S. preventive services task force recommendation. *Ann. Int. Med.* **164**(4), 279–296 (2016). doi:[10.7326/M15-2886](https://doi.org/10.7326/M15-2886)